Intravoxel incoherent motion magnetic resonance imaging for predicting the long-term efficacy of immune checkpoint inhibitors in patients with non-small-cell lung cancer

メタデータ	言語: eng 出版者: 公開日: 2021-06-01 キーワード (Ja): キーワード (En): 作成者: Karayama, Masato, Yoshizawa, Nobuko, Sugiyama, Masataka, Mori, Kazutaka, Yasui, Hideki , Hozumi, Hironao, Suzuki, Yuzo, Furuhashi, Kazuki, Fujisawa, Tomoyuki, Enomoto, Noriyuki, Nakamura, Yutaro, Inui, Naoki, Goshima, Satoshi, Suda, Takafumi, Takehara, Yasuo メールアドレス: 所属:
URL	http://hdl.handle.net/10271/00003773

This work is licensed under a Creative Commons Attribution-NonCommercial-ShareAlike 3.0 International License.

Intravoxel incoherent motion magnetic resonance imaging for predicting the long-term efficacy of immune checkpoint inhibitors in patients with non-small-cell lung cancer

Authors: Masato Karayama[1,2], Nobuko Yoshizawa[3], Masataka Sugiyama[4], Kazutaka Mori[5], Hideki Yasui[1], Hironao Hozumi[1], Yuzo Suzuki[1], Kazuki Furuhashi[1], Tomoyuki Fujisawa[1], Noriyuki Enomoto[1], Yutaro Nakamura[1], Naoki Inui[1, 6], Satoshi Goshima[3], Takafumi Suda[1], Yasuo Takehara[4]

Affiliations:

[1]Second Division, Department of Internal Medicine, Hamamatsu University School of Medicine, 1-20-1 Handayama, Hamamatsu 431-3192, Japan

[2]Department of Chemotherapy, Hamamatsu University School of Medicine, 1-20-1 Handayama, Hamamatsu 431-3192, Japan

[3]Department of Diagnostic Radiology and Nuclear Medicine, Hamamatsu University School of Medicine, 1-20-1 Handayama, Hamamatsu 431-3192, Japan

[4]Department of Fundamental Development for Advanced Low Invasive Diagnostic Imaging, Nagoya University, Graduate School of Medicine, 65 Tsurumai-cho,

Shouwa-ku, Nagoya 466-8550, Japan

[5]Department of Respiratory Medicine, Shizuoka City Shimizu Hospital, 1231 Miyakami, Shizuoka, 424-8636, Japan

[6]Department of Clinical Pharmacology and Therapeutics, Hamamatsu University School of Medicine, 1-20-1 Handayama, Hamamatsu 431-3192, Japan

Corresponding author: Masato Karayama MD, PhD

Hamamatsu University School of Medicine

1-20-1 Handayama, Hamamatsu 431-3192, Japan

Tel: +81-53-435-2263

Fax: +81-53-435-2386

E-mail: karayama@hama-med.ac.jp

Declarations of interest: None.

Abbreviations

ADC, apparent diffusion coefficient

ADC_{kurt}, kurtosis of ADC

ADC_{skew} , skewness of ADC

AUC, area under the curve

CI, confident interval

DWI-MRI, diffusion-weighted magnetic resonance imaging

ECOG, Eastern Cooperative Oncology Group

ICI, immune checkpoint inhibitor

IVIM-MRI, intravoxel incoherent motion magnetic resonance imaging

MRI, magnetic resonance imaging

NSCLC, non-small-cell lung cancer

OS, overall survival

PD, progressive disease

PD-1, programmed death-1

PD-L1, programmed death ligand-1

PFS, progression-free survival

PR, partial response

RECIST, Response Evaluation Criteria in Solid Tumors

ROC, receiver operating characteristic

ROI, region of interest

SD, stable disease

TPS, tumor proportion score

TTR, time to response

D, true diffusion coefficient

*D**, pseudodiffusion coefficient

f, perfusion fraction

Δ, change from the baseline

Abstract

Objectives: Conventional evaluation of anti-tumor activity on the basis of tumor size is inadequate for immune checkpoint inhibitors (ICIs). We therefore aimed to assess the usefulness of intravoxel incoherent motion magnetic resonance imaging (IVIM-MRI) for evaluation of the therapeutic efficacy of ICIs.

Materials and Methods: A chest IVIM-MRI was performed before and 2, 4, and 8 weeks after administration of ICIs in patients with advanced non-small-cell lung cancer. Apparent diffusion coefficient (ADC), skewness of ADC (ADC_{skew}), kurtosis of ADC (ADC_{kurt}), true diffusion coefficient (*D*), pseudodiffusion coefficient (*D**), and perfusion fraction (*f*) were evaluated at each evaluation point and changes from the baseline (Δ).

Results: Twenty patients were enrolled in this study. An increased ADC 8 weeks and decreased ADC_{kurt} and ΔADC_{kurt} 4 weeks after ICIs was associated with objective responses and longer progression-free survival (PFS). A decreased ΔADC_{skew} at 4 weeks was associated with objective responses, disease control, and longer PFS and overall survival. There was no correlation between the efficacy of ICIs and *D*, *D** and *f*. All of three patients who had pseudoprogression had decreased ΔADC_{skew} at 4 weeks

and two of them had decreased ΔADC_{kurt} at 4 weeks. Inversely, all five patients who had progressive disease (PD) did not have increased ΔADC_{skew} at 4 weeks and only one of them had decreased ΔADC_{kurt} at 4 weeks.

Conclusions: Changes in histograms of ADC may be useful for predicting long-term efficacy and distinguishing between pseudoprogression and actual PD after ICIs.

Keywords: IVIM-MRI, immune therapy, anti-programmed death-1 therapy, anti-PD-1 therapy, pseudoprogression, atypical radiologic response.

1. Introduction

Immune checkpoint inhibitors (ICIs) are emerging as a new treatment option for cancer therapy[1]. Unlike conventional cytotoxic chemotherapy, ICI does not cause cancer cell death directly, but rather alters cancer immunity and the tumor microenvironment [1–4]. With the increasingly widespread use of ICIs, an issue has emerged; namely, that conventional response criteria based on tumor size may not be adequate for evaluating anti-tumor activity and long-term efficacy of ICIs [5,6]. Compared with chemotherapy, ICIs achieve modest or sometimes no significant improvement in tumor response as assessed according to the Response Evaluation Criteria in Solid Tumors (RECIST); however, they achieve longer survival as determined by duration of response, progression-free survival (PFS), and/or overall survival (OS)[7,8].

In addition, ICIs have raised a new issue concerning radiological assessment. Patients receiving ICIs sometimes demonstrate delayed responses after an initial increase in tumor burden; this phenomenon has been called “pseudoprogression”. A transient increase in tumor size caused by edema and infiltration of immune cells, or a

delayed clinical response to ICIs are thought to be responsible for pseudoprogression[5,6,9]. To avoid incorrect diagnosis of pseudoprogression as true progression, iRECIST (a new guideline for response criteria for immunotherapies) has introduced the new category of unconfirmed progressive disease (iUPD), which requires confirmation by further increases in tumor size during ongoing immunotherapies. If progression is thus confirmed, the response category of confirmed progressive disease (iCPD) is assigned rather than iUPD [10]. However, the decision of iCPD requires at least two, and often more, evaluations. It is difficult to accurately distinguish pseudoprogression from true disease progression at the first evaluation by conventional radiological examinations. Thus, a new paradigm for radiological assessments is needed to assess the effects of ICIs with their unique anti-tumor mechanisms [6].

Diffusion-weighted magnetic resonance imaging (DWI-MRI) can provide qualitative and quantitative information about tumors, not just their size. DWI-MRI evaluates the random motion of water molecules, which is modified and limited by interactions with cell membranes and macromolecules in tissues [11,12]. Cancer tissues have dense cellularity and therefore restricted diffusion, which is reflected in low mean

apparent diffusion coefficients (ADCs). Effective cancer treatment results in decreased cellularity, loss of cell membrane integrity, increased extracellular space, and therefore, an increase in ADC [11,12]. Increased ADC reportedly correlates with tumor necrosis.[13]. Histograms of ADC, which reflect the heterogeneity of a tumor microenvironment, also change after cancer therapy[12,14]. Both changes in mean ADC and in histograms of ADC often precede changes in tumor size and are therefore useful for early prediction of efficacy of chemotherapy, radiotherapy, and chemoradiotherapy in various types of cancer.[15–17]. Furthermore, another recent advance in diagnostic radiology, intravoxel incoherent motion MRI (IVIM-MRI) can supply information about both tissue diffusion and microcapillary perfusion components [18–20]. IVIM-MRI provides information regarding the tumor microenvironments and is reportedly useful in monitoring and/or predicting efficacy of cancer treatments [19,21–24].

However, little is known about the changes in IVIM-MRI after administration of ICIs and their usefulness for evaluating their therapeutic efficacy. We hypothesized that pathological changes in the tumor microenvironment after ICIs can

be evaluated by IVIM-MRI. In the current study, we assessed chest IVIM-MRI before and after administration of ICIs and the association between identified changes and efficacy in patients with advanced non-small-cell lung cancer (NSCLC).

2. Patients and methods

2.1. Study design

This prospective observational study was conducted in accordance with the ethical standards described in the Declaration of Helsinki. The study protocol was approved by the Institutional Review Board of Hamamatsu University School of Medicine (No. 16-077). Each patient provided written informed consent to be included in the study. The study was registered with the University Hospital Medical Information Network Clinical Trial Registry (identification code: 000023462).

2.2. Patient eligibility

Patients with pathologically diagnosed non-small-cell lung cancer who were scheduled for anti-programmed death-1 (PD-1) therapy were eligible for inclusion. Major

inclusion criteria were age >18 years, Eastern Cooperative Oncology Group (ECOG) performance status 0–2, having inoperable stage IIIB or IV or recurrent disease, no prior history of immune checkpoint therapy, and having measurable lesions on chest MRI imaging with longest diameter of more than 1 cm. Exclusion criteria included uncontrolled brain metastasis, active interstitial lung disease, active autoimmune diseases, and other uncontrolled complications.

2.3. Evaluation schedule

Chest MRI was performed before and 2, 4, and 8 weeks after anti-PD-1 therapy. Anti-PD-1 therapy was administered as follows: nivolumab, 3 mg/kg every 2 weeks or pembrolizumab, 200mg every 3 weeks. Anti-PD-1 therapy was selected by the treating physician and continued until disease progression or unacceptable toxicity occurred. Chest CT was performed before and 4 and 8 weeks after initiating anti-PD-1 therapy and then repeated every 8 weeks during further anti-PD-1 therapy. Radiological response was evaluated according to RECIST version 1.1. Patients who demonstrated an initial increase in tumor burden (namely, iUPD defined by iRECIST), but

subsequently had evidence of delayed responses were recorded as having pseudoprogression[5,10].

2.4. Conventional MRI protocol

MR imaging was performed on a 3.0T MRI (Discovery MR750; GE Healthcare, Waukesha, WI, USA), using a torso array coil. The following parameters were employed for conventional fat-saturated T2–weighted imaging in all patients: fat-saturated T2-weighted fast spin-echo (TR/TE), 3000–5000/54 ms; imaging matrices, 320 × 320; FOV, 36 cm; parallel imaging factor, 3; section thickness, 5mm; and number of excitation of 4. The scan time was 2 min and 53 s.

2.5. IVIM-MRI

All patients underwent IVIM-MRI using the same MR scanner and torso array coil. The parameters used for diffusion weighted single-shot spin-echo based echo-planar imaging were TR/TE, 4000/53.8 ms; imaging matrices, 128 × 128; FOV, 40 cm; parallel imaging factor, 2; section thickness, 5 mm; *b* values, 0, 10, 20, 30, 50, 80, 100, 200, 400,

and 800 s/mm^2. The imaging time for IVIM-MRI was 448 s. The imaging was performed under shallow and quiet breathing to minimize the effect of respiratory motion.

2.6. Calculations of IVIM parameters

All analyses concerning IVIM were performed using image-analyzing software (SYNAPSE VINCENT; Fuji Film, Tokyo, Japan). The ADC value was calculated using the minimum and the maximum b values as follows:

ADC＝ln(S_0/S_{800})/(b800－b0), where S represents the signal intensity in the b value.

In the biexponential IVIM model, the relationship between signal variation and b values is expressed as follows:

$S_b/S_0 = (1 - f) \times \exp(-b \times D) + f \times \exp(-b \times D^*)$, where f is the fractional perfusion related to microcirculation, D is the true diffusion as reflected by pure molecular diffusion, and D^* is the pseudo-diffusion coefficient related to perfusion.

In addition, skewness of ADC (ADC_{skew}) and kurtosis of ADC (ADC_{kurt}) were calculated by histogram analysis (Figure 1). Skewness is a measure of the asymmetry of

distribution: being 0 with a normal (symmetrical) distribution, positive in a leftward distribution, and negative in a rightward distribution. Kurtosis is a measure of the peakedness and wideness of a distribution: kurtosis is higher in a peaked distribution and lower in a flattened distribution. Changes from the baseline (Δ) were also calculated at each evaluation point for each parameter. The largest of the measurable lesions was evaluated as the region of interest (ROI). Using fat-saturated T2-weighted images as reference, IVIM parameters were measured by drawing a ROI within the tumor that was as large as possible while excluding large vessels and areas with obvious susceptibility artifacts caused by air–water interfaces. ROIs were manually drawn in one slice (the largest tumor area slice). Two independent investigators evaluated the IVIM-MRI and the results are expressed as a mean of the two estimates.

2.7. Statistical analyses

The Wilcoxon signed rank test was used to evaluate changes from the baseline in IVIM data and the Wilcoxon rank sum test to compare IVIM data among responses to anti-PD-1 therapy. Logistic regression analysis was used to evaluate predictive factors

for objective response and disease control. Cox proportional hazard analysis was used to evaluate predictive factors for PFS and OS. Both PFS and OS were measured from the date of administration of anti-PD-1 therapy. Kaplan–Meier survival curves and log-rank tests were used to analyze PFS and OS. Time to response (TTR), defined as the time to the first objective response from initiating anti-PD-1 therapy, was evaluated in patients who achieved objective responses. Receiver operating characteristic (ROC) analysis was performed to estimate the cut-off values for IVIM-MRI parameters for objective response and disease control. Cut-off values were determined using Youden's index (maximum value of [sensitivity + specificity − 1]). Time-dependent ROC analysis was performed to estimate the cut-off values for IVIM-MRI parameters for PFS and OS. A p value <0.05 (two-sided) was considered to denote significance. All values were analysed using JMP v13.0.0 (SAS Institute Japan, Tokyo, Japan), except for time-dependent ROC analyses, for which R version 3.5.3 was used (R Foundation for Statistical Computing, Vienna, Austria, 2019) with additional packages (survivalROC).

3. Results

3.1. Patient characteristics

From June 2016 to December 2018, 20 patients were enrolled in the study. Table 1 shows their baseline characteristics. The median age was 68 years (range, 40–82 years) and 16 patients (80.0%) were male. Fifteen patients (75.0%) had a history of smoking. Most of the patients had good performance status, with ECOG performance status of 0 or 1 (n=19, 95.0%). Seventeen patients (85.0%) had stage IV disease. Thirteen patients (65.0%) had a histological diagnosis of adenocarcinoma and five (25.0%) had squamous cell carcinoma. Fourteen patients (70.0%) showed programmed death-ligand 1 (PD-L1) expression on immunohistochemistry with tumor proportion scores (TPS) of ≥1% (22C3 pharmDX Dako; Agilent, Santa Clara, CA, USA), and eight (40.0%) had high expression with TPS of ≥50%. Only one patient had active gene mutation, namely *epidermal growth factor receptor* gene mutation with exon 19 deletion. The median follow-up time was 10.0 months (range, 3.0–22.3 months).

3.2. Efficacy of immune checkpoint inhibitor therapy

Seven patients (35.0%) received pembrolizumab as first line therapy and thirteen (65.0%) received nivolumab as second line or later therapy. The best responses to anti-PD-1 therapy were progressive disease (PD) in five patients (25.0%), stable disease (SD) in six (30.0%), and partial response (PR) in nine (45.0%), yielding an objective response rate of 45.0% and disease control rate of 75%. The median PFS was 9.7 months (95% confident interval [CI], 1.6–18.1 months) and the median OS was 11.8 months (95% CI, 6.7–14.0 months). The median TTR of the nine patients who achieved objective responses was 6.1 weeks (95% CI, 3.6–12.2 weeks)

Changes in IVIM-MRI according to response to immune checkpoint inhibitor therapy

Seventeen patients completed MRI measurements at all four specified time points. One of these patients had no measurable lesions at 8 weeks because of a good response to anti-PD-1 therapy. Three patients could not complete the preplanned MRI measurements at 8 weeks because anti-PD-1 therapy had been discontinued as a result of disease progression.

The results of ADC, ADC_{skew}, and ADC_{kurt} according to the responses to ICIs

are shown in Figure 2A-F. Patients who achieved PR had significantly increased ADC at 8 weeks (1.73 p=0.043) and decreased ADC_{skew} at 4 and 8 weeks (0.37, p=0.012; and 0.12, p=0.019, respectively) compared with baseline (1.28, and 0.85, respectively) (Figure 2A, C). In contrast, patients with PD demonstrated non-significant decreases in ADC at 8 weeks (1.46, p=0.423), and non-significant increases in ADC_{skew} at 4 and 8 weeks (0.79, p=0.059; and 0.54, p=0.523, respectively) compared with baseline (1.50, and 0.40, respectively). Patients with SD demonstrated no significant changes in ADC, ADC_{skew}, and ADC_{kurt}. There were no significant changes in D, D^* and f (Supplementary Table 1). The histograms of ADC of representative patients with PR, PD, and pseudoprogression are shown in Figure 1A, B, and C, respectively.

3.3. Predictors in IVIM-MRI for response to immune checkpoint inhibitor therapy

At baseline and 2 weeks after initiating ICI therapy, there were no significant differences in IVIM data between patients who had PD, SD, and PR. At 4 weeks after ICI therapy, patients who had achieved PR demonstrated significantly lower ADC_{skew} (0.12, p=0.016), ΔADC_{skew} (−0.46, p=0.034), ADC_{kurt} (3.41, p=0.023), and ΔADC_{kurt}

(−0.90, p=0.033) than those who had PD (0.79, 0.39, 4.76, and 1.44, respectively) (Figure 2C-F). Patients who had SD also demonstrated significantly lower ADC_{skew} (-0.40×10^{-2}, p=0.008) and ADC_{kurt} (3.10, p=0.008), and a non-significant lower ΔADC_{skew} (−0.35, p=0.083) and ΔADC_{kurt} (−0.45 p=0.055) at 4 weeks than patients who had PD (Figure 2C-F). At 8 weeks, patients who had PR and SD demonstrated non-significant lower ADC_{skew}, ΔADC_{skew}, ADC_{kurt}, and ΔADC_{kurt} than those who had PD. There were no significant differences in other IVIM parameters among the responses to ICIs (Supplementary Table 1).

Among IVIM data, ΔADC at 8 weeks, and ΔADC_{skew} at 4 and 8 weeks were significant predictors of objective response (p=0.026, p=0.034 and 0.028, respectively) (Table 2 and Supplementary Table 2). The cut-off values for objective response were ΔADC of 0 at 8 weeks (sensitivity 0.88, specificity 0.75, and area under the curve [AUC] 0.81), ΔADC_{skew} of −0.01 at 4 weeks (sensitivity 1.00, specificity 0.73, and AUC 0.79) and −0.11 at 8 weeks (sensitivity 0.88, specificity 0.75, and AUC 0.83). ADC_{skew}, ΔADC_{skew}, ADC_{kurt}, and ΔADC_{kurt} at 4 weeks were significant predictors of disease control (p<0.001, 0.001, <0.001, and 0.003, respectively) (Table 2). The cut-off

values for disease control were ADC_{skew} of 0.65 (sensitivity 1.00, specificity 0.80, and AUC 0.95), ΔADC_{skew} of −0.01 (sensitivity 0.80, specificity 1.00, and AUC 0.93), ADC_{kurt} of 3.91 (sensitivity 0.80, specificity 1.00, and AUC 0.93), and ΔADC_{kurt} of 0.34 (sensitivity 0.93, specificity 0.80, and AUC 0.87) at 4weeks. High PD-L1 expression of TPS ≥50% and first-line treatment with anti-PD-1 therapy were significant predictors of objective response (p<0.001, and 0.004, respectively) and disease control (p=0.023, and 0.014, respectively). Objective response at 4 weeks according to RECIST was not a significant predictor of overall response.

3.4. Predictors in IVIM-MRI for PFS and OS after immune checkpoint inhibitor therapy

According to univariate Cox proportional hazard analyses, increased ΔADC at 8 weeks and decreased ΔADC_{skew}, ADC_{kurt}, and ΔADC_{kurt} at 4 weeks were significant predictors of longer PFS (p=0.016, 0.043, 0.008, and 0.028, respectively), as were high PD-L1 expression of TPS ≥1%, ≥50%, first-line treatment, and overall objective response (p=0.038, <0.001, 0.029, and 0.001, respectively) (Table 2 and

Supplementary Table 2). Decreased ΔADC_{skew} at 4 weeks and overall objective response were significant predictors of OS (p=0.042 and 0.008, respectively). Objective response at 4 weeks according to RECIST was not a significant predictor factor of PFS nor OS.

Time-dependent ROC analyses for PFS identified cut-off values for ΔADC at 8 weeks, ΔADC_{skew}, ADC_{kurt}, and ΔADC_{kurt} at 4 weeks of −0.28, −0.01, 3.91, and 0.34, respectively (Supplementary Figure 1). PFS curves based on the cut-off values are shown in Figure 3A-D. Patients with decreased ΔADC_{skew} <−0.01, ADC_{kurt} <3.91, and ΔADC_{kurt} <0.34 at 4 weeks demonstrated significantly longer PFS (10.4 months, 95% CI, 5.4–18.1 months; 18.1 months, 95% CI, 5.4–18.1 months; and 9.7 months, 95% CI, 5.4–18.1 months; respectively) compared with those without these changes (1.6 months, 95% CI, 0.8 months–not estimable [N.E.], p<0.001; 1.6 months, 95% CI, 0.8–10.4 months, p=0.020; and 1.1 months, 95% CI, 0.8 months–N.E. p=0.004; respectively) (Figure 3B-D). Patients with increased ΔADC >−$0.28\times10^{-3}mm^2$/sec at 8 weeks demonstrated longer PFS (9.7 months, 95% CI, 5.4–18.1 months), compared without increased ΔADC >−$0.28\times10^{-3}mm^2$/sec at 8 weeks; this difference was of

borderline significance (3.5 months, 95% CI, 1.6–5.4 months, p=0.051) (Figure 3A).

Time-dependent ROC analyses for OS identified cut-off values for ΔADC at 8 weeks, ΔADC_{skew}, ADC_{kurt}, and ΔADC_{kurt} at 4 weeks of −0.01, 0.01, 4.00, and 1.82, respectively (Supplementary Figure 1). OS curves based on the cut-off values are shown in Figure 3E-H. Patients with decreased ΔADC_{skew} <0.01 at 4 weeks demonstrated significantly longer median OS of 14.0 months (95% CI, 9.6–19.5 months), compared with those with ΔADC_{skew} ≥0.01 of 5.2 months (95% CI, 3.1–12.4 months, p=0.003) (Figure 3F). There were no significant differences in OS for the other IVIM-MRI parameters.

3.5. Pseudoprogression and changes in IVIM-MRI

Three patients demonstrated pseudoprogression and five patients "true" PD. All three patients with pseudoprogression had decreased ΔADC_{skew} at 4 weeks and two of them had decreased ΔADC_{kurt} at 4 weeks (Table 3 and Supplementary Figure 2). In contrast, all five patients with PD did not have decreased ΔADC_{skew} at 4 weeks and only one had decreased ΔADC_{kurt} at 4 weeks. As to the results, decreased ΔADC_{skew} <−0.14 at 4

weeks yielded a 100% sensitivity (95% CI, 19.4%–100%) and a 100.0% specificity (95% CI, 35.9%–100%), and decreased ΔADC_{kurt} <−0.69 at 4 weeks yielded a 66.7% sensitivity (95% CI, 9.4%–99.2%) and a 80.0% specificity (95%CI, 28.4%–99.5%) for detection of pseudoprogression.

4. Discussion

In the current study, we evaluated chest IVIM-MRI before and after ICI therapy in patients receiving ICI therapy for NSCLC. We found that of the examined IVIM-MRI parameters, changes in mean ADC and histogram of ADC were associated with the efficacy of ICI therapy as follows: 1) increased mean ADC 8 weeks after initiating anti-PD-1 therapy was associated with objective response and a longer PFS; 2) deceased ΔADC_{skew} at 4 weeks was associated with objective response, disease control, and longer PFS and OS; and 3) decreased ADC_{kurt} and ΔADC_{kurt} at 4 weeks were associated with disease control and longer PFS. In addition, decreased ΔADC_{skew} and ΔADC_{kurt} at 4 weeks demonstrated considerable sensitivity and specificity in distinguishing pseudoprogression from “true” disease progression. Assessments of

chest IVIM-MRI may be useful for predicting efficacy and for distinguishing between pseudoprogression and true progression after anti-PD-1 therapy in patients with NSCLC.

Changes in the histogram of ADC may reflect changes in the heterogeneity of the tumor microenvironment in response to ICIs. A decreased ΔADC_{skew} represents a right shift of the histogram, in other words, a greater proportion of pixels have high ADC (Figure 1). A decreased ADC_{kurt} represents a decreased peak of the histogram, which means resolution of a concentrated distribution in a limited range of ADC (Figure 1). A right shift and a decreased peak of ADC are reported to occur after effective cancer treatment with non-ICI agents [15,16,25]. Changes in cellularity, membrane integrity, and extracellular space may result in changes in histograms of ADC. In addition, expression of PD-L1, a target of anti-PD-1/PD-L1 therapy, is spatially heterogeneous within a tumor [26–28]. Cancer genomic analysis in patients with melanoma receiving nivolumab has shown that changes in intratumoral heterogeneity are related to therapeutic efficacy, responders frequently having fewer clonal variants, whereas in non-responders clonal variants are unchanged or even

increased [2]. It is possible that heterogeneous intratumoral expression of PD-L1 results in heterogeneous anti-tumor response to ICIs, which may result in changes in the distribution of ADC.

Changes in the histograms of ADC after ICIs precede increases in mean ADC. An increased mean ADC reflects decreased cellularity after cancer treatment and is therefore associated with the efficacy of several cancer therapies in various cancer types [29–34]. Also, in the current study, patients who achieved PR had increased mean ADC 8 weeks after initiating anti-PD-1 therapy, but not at 4 weeks. In contrast, ADC_{skew} was decreased at 4 weeks; this change preceded the median TTR of 6.1 weeks determined by conventional CT assessment (Table 3). Changes in mean ADC indicate changes in whole tumors, whereas those in histograms of ADC may indicate partial changes in tumors. Therefore, changes in histograms of ADC may indicate subtle immune responses triggered by ICIs that are not detected by the less sensitive mean ADC and conventional CT.

In addition to early prediction, changes in histograms of ADC may provide additional information about the efficacy of ICI therapy that is not detectable by

conventional means of identifying objective responses according to RECIST. Unlike conventional chemotherapy, ICIs enhance antitumor immune responses, which leads to therapeutic benefits that do not always manifest as short-term reductions in tumor size. Therefore, SD may be considered a meaningful therapeutic effect and even PD as determined by radiologic evaluation does not necessarily reflect therapeutic failure in immunotherapy [5,35,36]. In the current study, of the patients who did not achieve objective responses, those with decreased $\Delta ADC_{skew} < -0.01$ at 4 weeks demonstrated relatively long PFS and OS (5.4 and 11.8 months, respectively), whereas those with $\Delta ADC_{skew} \geq -0.01$ had PFS and OS of 1.6 and 5.9 months, respectively. Furthermore, decreased ΔADC_{skew} and ΔADC_{kurt} were also observed in patients with pseudoprogression. Changes in histograms of ADC may occur irrespective of a transient increase in tumor size and detect true responses to ICI therapy.

The other assessed IVIM-MRI parameters, *D*, *D**, and *f*, did not correlate with the efficacy of ICIs. These parameters are thought to reflect microcapillary perfusion and therefore correlate with the efficacy of anti-vascular therapy [23]. The ICIs have little direct effect on the vascular microenvironment and did not alter

vascular perfusion-related factors in the current study. IVIM-MRI is reportedly useful in assessing non-ICI therapy for bone metastases, nasopharyngeal carcinoma, and breast cancer [19,21,24]. It is possible that there are cancer type-specific differences in changes in IVIM-MRI parameters after cancer therapy.

The current study had four main limitations. First, it is possible that there was some influence of respiratory motion on chest MRI. To minimize the effect of respiratory motion, MRI imaging was performed with the patient breathing shallowly and quietly. Additionally, the largest of the measurable lesions was designated as the ROI to further minimize the effects of respiratory motion. Second, we did not adjust associations between histograms of ADC and efficacy of ICIs by potential confounding factors because of the limited number of study patients. Pathology, tumor expression of PD-L1, and ECOG performance status are known to be associated with the efficacy of ICIs [7,8,37,38]. Third, we only evaluated single therapy with anti-PD-1 antibodies. Novel strategies involving immune checkpoint therapy have recently emerged for several cancers, such as anti-PD-L1 antibody, combination therapy with two different ICIs (e.g. anti-PD-1 antibody and anti-cytotoxic T-lymphocyte associated antigen-4

antibody), and combined chemotherapy and ICIs [8,39,40]. Fourth, it is unknown whether changes in histogram of ADC would also occur after treatment of different cancer types besides NSCLC. Further studies are required with a larger number of patients with different types of cancers receiving immunotherapies to validate the usefulness of histogram of ADC.

Conclusions

In patients with NSCLC, changes in histograms of ADC may be useful for predicting long-term efficacy and distinguishing between pseudoprogression and true PD after ICIs.

Acknowledgments: The authors thank Naoki Oishi, R.T. and Masanori Kawate, R.T. for technological assistance and Dr Trish Reynolds, MBBS, FRACP, from Liwen Bianji, Edanz Group China (www.liwenbianji.cn/ac), for editing the English text of a draft of this manuscript.

Funding: This research did not receive any specific grant from funding agencies in the public, commercial, or not-for-profit sectors.

References

[1] D.M. Pardoll, The blockade of immune checkpoints in cancer immunotherapy, Nat. Rev. Cancer. 12 (2012) 252–264. doi:10.1038/nrc3239.

[2] N. Riaz, J.J. Havel, V. Makarov, A. Desrichard, W.J. Urba, J.S. Sims, et al., Tumor and Microenvironment Evolution during Immunotherapy with Nivolumab, Cell. 171 (2017) 934-949.e15. doi:10.1016/j.cell.2017.09.028.

[3] P.C. Tumeh, C.L. Harview, J.H. Yearley, I.P. Shintaku, E.J.M. Taylor, L. Robert, et al., PD-1 blockade induces responses by inhibiting adaptive immune resistance, Nature. 515 (2014) 568–571. doi:10.1038/nature13954.

[4] J.L. da Silva, A.L.S. Dos Santos, N.C.C. Nunes, F. de Moraes Lino da Silva, C.G.M. Ferreira, A.C. de Melo, Cancer immunotherapy: the art of targeting the tumor immune microenvironment, Cancer Chemother. Pharmacol. 84 (2019) 227–240. doi:10.1007/s00280-019-03894-3.

[5] J.D. Wolchok, A. Hoos, S. O'Day, J.S. Weber, O. Hamid, C. Lebbé, et al., Guidelines for the evaluation of immune therapy activity in solid tumors: Immune-related response criteria, Clin. Cancer Res. 15 (2009) 7412–7420.

doi:10.1158/1078-0432.CCR-09-1624.

[6] M. Nishino, H. Hatabu, F.S. Hodi, Imaging of cancer immunotherapy: Current approaches and future directions, Radiology. 290 (2019) 9–22. doi:10.1148/radiol.2018181349.

[7] H. Borghaei, L. Paz-Ares, L. Horn, D.R. Spigel, M. Steins, N.E. Ready, et al., Nivolumab versus docetaxel in advanced nonsquamous non-small-cell lung cancer, N. Engl. J. Med. 373 (2015) 1627–1639. doi:10.1056/NEJMoa1507643.

[8] A. Rittmeyer, F. Barlesi, D. Waterkamp, K. Park, F. Ciardiello, J. von Pawel, et al., Atezolizumab versus docetaxel in patients with previously treated non-small-cell lung cancer (OAK): a phase 3, open-label, multicentre randomised controlled trial, Lancet. 389 (2017) 255–265. doi:10.1016/S0140-6736(16)32517-X.

[9] V.L. Chiou, M. Burotto, Pseudoprogression and immune-related response in solid tumors, J. Clin. Oncol. 33 (2015) 3541–3543. doi:10.1200/JCO.2015.61.6870.

[10] L. Seymour, J. Bogaerts, A. Perrone, R. Ford, L.H. Schwartz, S. Mandrekar, et

al., iRECIST: guidelines for response criteria for use in trials testing immunotherapeutics, Lancet Oncol. 18 (2017) e143–e152. doi:10.1016/S1470-2045(17)30074-8.iRECIST.

[11] D.M. Koh, D.J. Collins, Diffusion-weighted MRI in the body: Applications and challenges in oncology, Am. J. Roentgenol. 188 (2007) 1622–1635. doi:10.2214/AJR.06.1403.

[12] A.R. Padhani, G. Liu, D. Mu-Koh, T.L. Chenevert, H.C. Thoeny, T. Takahara, et al., Diffusion-weighted magnetic resonance imaging as a cancer biomarker: Consensus and recommendations, Neoplasia. 11 (2009) 102–125. doi:10.1593/neo.81328.

[13] M. Chiaradia, L. Baranes, J.T. Van Nhieu, A. Vignaud, A. Laurent, T. Decaens, et al., Intravoxel incoherent motion (IVIM) MR imaging of colorectal liver metastases: Are we only looking at tumor necrosis?, J. Magn. Reson. Imaging. 39 (2014) 317–325. doi:10.1002/jmri.24172.

[14] B.A. Moffat, D.E. Hall, J. Stojanovska, P.J. McConville, J.B. Moody, T.L. Chenevert, et al., Diffusion imaging for evaluation of tumor therapies in

preclinical animal models, Magn. Reson. Mater. Physics, Biol. Med. 17 (2004) 249–259. doi:10.1007/s10334-004-0079-z.

[15] M. Nowosielski, W. Recheis, G. Goebel, Ö. Güler, G. Tinkhauser, H. Kostron, et al., ADC histograms predict response to anti-angiogenic therapy in patients with recurrent high-grade glioma, Neuroradiology. 53 (2011) 291–302. doi:10.1007/s00234-010-0808-0.

[16] S. Kyriazi, D.J. Collins, C. Messiou, R.L. Davidson, S.L. Giles, S.B. Kaye, et al., Metastatic ovarian and primary peritoneal cancer : assessing chemotherapy response with diffusion-weighted MR imaging - value of histogram analysis of apparent diffusion coefficients, Radiology. 261 (2011) 182–192.

[17] R.F. Barajas, J.L. Rubenstein, J.S. Chang, J. Hwang, S. Cha, Diffusion-weighted MR imaging derived apparent diffusion coefficient is predictive of clinical outcome in primary central nervous system lymphoma, Am. J. Neuroradiol. 31 (2010) 60–66. doi:10.3174/ajnr.A1750.

[18] V. Lai, X. Li, V.H.F. Lee, K.O. Lam, Q. Chan, P.L. Khong, Intravoxel incoherent motion MR imaging: Comparison of diffusion and perfusion

characteristics between nasopharyngeal carcinoma and post-chemoradiation fibrosis, Eur. Radiol. 23 (2013) 2793–2801. doi:10.1007/s00330-013-2889-8.

[19] M. Gaeta, C. Benedetto, F. Minutoli, T. D'Angelo, E. Amato, S. Mazziotti, et al., Use of diffusion-weighted, intravoxel incoherent motion, and dynamic contrast-enhanced MR imaging in the assessment of response to radiotherapy of lytic bone metastases from breast cancer, Acad. Radiol. 21 (2014) 1286–1293. doi:10.1016/j.acra.2014.05.021.

[20] D. Le Bihan, What can we see with IVIM MRI?, Neuroimage. 187 (2019) 56–67. doi:10.1016/j.neuroimage.2017.12.062.

[21] Y. Xiao-Ping, H. Jing, L. Fei-Ping, H. Yin, L. Qiang, W. Lanlan, et al., Intravoxel incoherent motion MRI for predicting early response to induction chemotherapy and chemoradiotherapy in patients with nasopharyngeal carcinoma, J. Magn. Reson. Imaging. 43 (2016) 1179–1190. doi:10.1002/jmri.25075.

[22] Z. Guo, Q. Zhang, X. Li, Z. Jing, Intravoxel incoherent motion diffusion weighted MR imaging for monitoring the instantly therapeutic efficacy of radiofrequency ablation in rabbit VX2 tumors without evident links between

conventional perfusion weighted images, PLoS One. 10 (2015) 1–14. doi:10.1371/journal.pone.0127964.

[23] I. Joo, J.M. Lee, J.K. Han, B.I. Choi, Intravoxel incoherent motion diffusion-weighted MR imaging for monitoring the therapeutic efficacy of the vascular disrupting agent CKD-516 in rabbit VX2 liver tumors1, Radiology. 272 (2014) 417–426. doi:10.1148/radiol.14131165.

[24] E.E. Sigmund, G.Y. Cho, S. Kim, M. Finn, M. Moccaldi, J.H. Jensen, et al., Intravoxel incoherent motion imaging of tumor microenvironment in locally advanced breast cancer, Magn. Reson. Med. 65 (2011) 1437–1447. doi:10.1002/mrm.22740.

[25] T.E. Yankeelov, M. Lepage, A. Chakravarthy, E.E. Broome, K.J. Niermann, M.C. Kelley, et al., Integration of quantitative DCE-MRI and ADC mapping to monitor treatment response in human breast cancer: initial results, Magn. Reson. Imaging. 25 (2007) 1–13. doi:10.1016/j.mri.2006.09.006.

[26] D.J. Pinato, R.J. Shiner, S.D.T. White, J.R.M. Black, P. Trivedi, J. Stebbing, et al., Intra-tumoral heterogeneity in the expression of programmed-death (PD)

ligands in isogeneic primary and metastatic lung cancer: Implications for immunotherapy, Oncoimmunology. 5 (2016) 1–7. doi:10.1080/2162402X.2016.1213934.

[27] S. Nakamura, K. Hayashi, Y. Imaoka, Y. Kitamura, Y. Akazawa, K. Tabata, et al., Intratumoral heterogeneity of programmed cell death ligand-1 expression is common in lung cancer, PLoS One. 12 (2017) 1–13. doi:10.1371/journal.pone.0186192.

[28] K. Yoshimura, Y. Inoue, M. Karayama, K. Tsuchiya, K. Mori, Y. Suzuki, et al., Heterogeneity analysis of PD-L1 expression and copy number status in EBUS-TBNA biopsy specimens of non-small cell lung cancer: Comparative assessment of primary and metastatic sites, Lung Cancer. 134 (2019) 202–209. doi:10.1016/j.lungcan.2019.06.002.

[29] M. Xie, W. Wang, S. Dou, L. Cui, W. Xiao, Quantitative computed tomography measurements of emphysema for diagnosing asthma-chronic obstructive pulmonary disease overlap syndrome., Int. J. Chron. Obstruct. Pulmon. Dis. 11 (2016) 953–61. doi:10.2147/COPD.S104484.

[30] C.Y. Chen, C.W. Li, Y.T. Kuo, T.S. Jaw, D.K. Wu, J.C. Jao, et al., Early response of hepatocellular carcinoma to transcatheter arterial chemoembolization: Choline levels and MR diffusion constants - Initial experience, Radiology. 239 (2006) 448–456. doi:10.1148/radiol.2392042202.

[31] V.N. Harry, S.I. Semple, F.J. Gilbert, D.E. Parkin, Diffusion-weighted magnetic resonance imaging in the early detection of response to chemoradiation in cervical cancer, Gynecol. Oncol. 111 (2008) 213–220. doi:10.1016/j.ygyno.2008.07.048.

[32] T. Tsuchida, M. Morikawa, Y. Demura, Y. Umeda, H. Okazawa, H. Kimura, Imaging the early response to chemotherapy in advanced lung cancer with diffusion-weighted magnetic resonance imaging compared to fluorine-18 fluorodeoxyglucose positron emission tomography and computed tomography, J. Magn. Reson. Imaging. 38 (2013) 80–88. doi:10.1002/jmri.23959.

[33] M.D. Pickles, P. Gibbs, M. Lowry, L.W. Turnbull, Diffusion changes precede size reduction in neoadjuvant treatment of breast cancer, Magn. Reson. Imaging. 24 (2006) 843–847. doi:10.1016/j.mri.2005.11.005.

[34] Y.S. Sun, X.P. Zhang, L. Tang, J.F. Ji, J. Gu, Y. Cai, et al., Locally advanced rectal carcinoma treated with preoperative chemotherapy and radiation therapy: Preliminary analysis of diffusion-weighted MR imaging for early detection of tumor histopathologic downstaging, Radiology. 254 (2010) 170–178. doi:10.1148/radiol.2541082230.

[35] F.S. Hodi, W.J. Hwu, R. Kefford, J.S. Weber, A. Daud, O. Hamid, et al., Evaluation of immune-related response criteria and RECIST v1.1 in patients with advanced melanoma treated with Pembrolizumab, J. Clin. Oncol. 34 (2016) 1510–1517. doi:10.1200/JCO.2015.64.0391.

[36] R. Thomas, B. Somarouthu, F. Alessandrino, K. Vikram, A.B. Shinagare, Atypical response patterns in patients treated with nivolumab, Am. J. Roentgenol. 212 (2019) 1177–1181.

[37] J. Brahmer, K.L. Reckamp, P. Baas, L. Crinò, W.E.E. Eberhardt, E. Poddubskaya, et al., Nivolumab versus docetaxel in advanced squamous-cell non-small-cell lung cancer, N. Engl. J. Med. 373 (2015) 123–135. doi:10.1056/NEJMoa1504627.

[38] D. Fujimoto, H. Yoshioka, Y. Kataoka, T. Morimoto, Y. Kim, K. Tomii, et al., Efficacy and safety of nivolumab in previously treated patients with non-small cell lung cancer: A multicenter retrospective cohort study., Lung Cancer. 119 (2018) 14–20. doi:10.1016/j.lungcan.

[39] J. Larkin, V. Chiarion-Sileni, R. Gonzalez, J.J. Grob, C.L. Cowey, C.D. Lao, et al., Combined nivolumab and ipilimumab or monotherapy in untreated Melanoma, N. Engl. J. Med. 373 (2015) 23–34. doi:10.1056/NEJMoa1504030.

[40] L. Gandhi, D. Rodríguez-Abreu, S. Gadgeel, E. Esteban, E. Felip, F. De Angelis, et al., Pembrolizumab plus chemotherapy in metastatic non-small-cell lung cancer, N. Engl. J. Med. 378 (2018) 2078–2092. doi:10.1056/NEJMoa1801005.

Figure legends

Figure 1: Histograms of apparent diffusion coefficient in representative patients after administration of immune checkpoint inhibitor therapy

(A) A patient with objective response demonstrated decreased skewness (rightward shift) and decreased kurtosis (downward and flattened shift) of apparent diffusion coefficient (ADC) 2 and 4 weeks after immune checkpoint therapy (ICI). (B) A patient with progressive disease demonstrated increased skewness (leftward shift) and increased kurtosis (upward and peaked shift) of ADC 2 and 4 weeks after ICI. (C) A patient with pseudoprogression demonstrated decreased skewness and kurtosis at 2 weeks, whereas a lung metastasis increased (arrow) and bilateral pleuritis (arrowheads) worsened. At 8 weeks, skewness and kurtosis were further decreased, the lung metastasis had diminished in size, and the bilateral pleuritis had improved.

Regions of interest are bordered by white lines in fat-saturated T2-weighted magnetic resonance images (fsT2WI) and ADC maps.

Figure 2: Changes in histograms of apparent diffusion coefficient after administration of immune checkpoint inhibitor therapy

(A) Time course of apparent diffusion coefficient (ADC), (B) changes from the baseline (Δ) of ADC, (C) skewness of ADC (ADC_{skew}), (D) ΔADC_{skew}, (E) kurtosis of ADC (ADC_{kurt}), and (F) ΔADC_{kurt} 2, 4, and 8 weeks after immune checkpoint inhibitor therapy. Black squares, progressive disease (PD); white triangles, stable disease (SD); grey filled circles, partial response (PR); black filled circles, pseudoprogression.

Figure 3: Progression-free and overall survival

Progression-free survival (PFS) according to (A) changes in apparent diffusion coefficient (ΔADC) at 8 weeks, (B) changes in skewness of ADC (ΔADC_{skew}) at 4 weeks, (C) kurtosis of ADC (ADC_{kurt}) at 4 weeks, and (D) ΔADC_{kurt} at 4 weeks. The cut-off values were $-0.28\times10^{-3}mm^2/sec$, −0.01, 3.91 and 0.34 respectively. Overall survival (OS) according to (E) ΔADC at 8 weeks, (F) ΔADC_{skew} at 4 weeks, (G) ADC_{kurt} at 4 weeks, and (H) ΔADC_{kurt} at 4 weeks. The cut-off values were $-0.01\times10^{-3}mm^2/sec$, 0.01, 4.00, and 1.82, respectively. The cut-off values were

determined by time-dependent receiver operating characteristic analysis (Supplementary Figure 1).

Table.1. Patient characteristics

	N=20
Age	68 (40 − 82)
Sex, male	16 (80.0)
Smoking status, never- / ever-smoker	5 (25.0) / 15 (75.0)
ECOG-PS, 0/1/2	9 (45.0) / 10 (50.0) / 1 (5.0)
Stage, IIIb / IV	3 (15.0) / 17 (85.0)
Pathology, adeno / squamous / others	13 (65.0) / 5 (25.0) / 2 (10.0)
PD-L1 expression,	
unknown or <1% / ≥1 −<50% / ≥50%	6 (30.0) / 6 (30.0) / 8 (40.0)
EGFR mutation, wild type / del 19	19 (95.0) / 1 (5.0)
ALK fusion gene, none / unknown	18 (90.0) / 2 (10.0)
Treatment line, 1st / ≥2nd	7 (35.0) / 13 (65.0)
Treatment, nivolumab / pembrolizumab	13 (65.0) / 7 (35.0)
Best response to anti-PD-1 therapy	
PD / SD / PR / CR	5 (25.0) / 6 (30.0) / 9 (45.0) / 0 (0)

Data are expressed as median (range) or number (%).

ALK, anaplastic lymphoma kinase; CR, complete response; ECOG-PS, Eastern Cooperative Oncology Group performance status; EGFR, epidermal growth factor receptor; PD-1, programmed cell death-1; PD-L1, programmed cell death-ligand 1; PD, progressive disease; PR, partial response; SD, stable disease.

Table 2. Univariate logistic regression and Cox proportional hazard analyses of factors associated with the efficacy of immune checkpoint inhibitor therapy

	Objective response		Disease control		Progression-free survival		Overall survival	
Variables	Odds ratio	*p*-value	Odds ratio	*p*-value	Hazard ratio	*p*-value	Hazard ratio	*p*-value
Pathology, squamous cell (vs. non-squamous)	4.00 (0.46 − 87.89)	0.221	7.60×10^{7} (1.04 – N.E.)	0.047	0.73 (0.11 − 2.95)	0.682	0.76 (0.25 − 2.84)	0.663
PD-L1 expression								
TPS≥1%	8.00 (0.99 – 1.74×10^{2})	0.051	4.00 (0.36 – 47.88)	0.246	0.23 (0.05 – 0.92)	0.038	0.66 (0.23 − 2.01)	0.449
TPS≥50%	38.50 (4.06 – 9.91×10^{2})	<0.001	7.53×10^{7} (1.53 – N.E)	0.023	0.06 (3.35×10^{-3} – 0.37)	<0.001	0.34 (0.08 − 1.08)	0.070

Treatment line, 1st (vs. ≥2nd)	22.00 (2.51 − 5.15×10^{2})	0.004	2.22×10^{7} (1.88 – N.E.)	0.014	0.22 (0.03 – 0.87)	0.029	0.59 (0.13 − 1.89)	0.395
Overall objective response					0.06 (0.32×10^{-2} – 0.36)	0.001	0.12 (0.02 − 0.48)	0.008
ΔADC[∫]								
at 2 weeks	1.26 (0.06 − 29.83)	0.874	0.90 (0.03 − 27.80)	0.950	1.18 (0.21 – 6.19)	0.834	2.74 (0.60 − 13.53)	0.200
at 4 weeks	1.26 (0.08 − 21.72)	0.862	7.37 (0.38 – 3.25×10^{2})	0.189	0.46 (0.10 – 2.81)	0.381	1.51 (0.46 – 6.06)	0.512
at 8 weeks	48.61 (1.51 – 8.88×10^{3})	0.026	1.93×10^{2} (0.84 – 2.71×10^{6})	0.060	0.07 (0.57×10^{-2} – 0.62)	0.016	0.50 (0.09 − 2.70)	0.415

ADC_{skew}[§]								
at baseline	5.72 (0.91 −77.01)	0.064	1.70 (0.27 −15.71)	0.583	0.62 (0.21 – 1.68)	0.353	0.79 (0.34 − 1.84)	0.587
at 2 weeks	1.51 (0.28 − 9.15)	0.628	1.35 (0.19 − 9.60)	0.756	0.51 (0.18 – 1.37)	0.178	0.63 (0.24 − 1.65)	0.342
at 4 weeks	0.54 (0.07 − 3.59)	0.526	2.38×10^{-6} (1.85×10^{-16} – 0.03)	<0.001	2.37 (0.56 – 12.47)	0.248	2.41 (0.74 − 9.49)	0.150
at 8 weeks	0.19 (0.05×10^{-1} – 1.86)	0.169	0.02 (1.85×10^{-5} – 1.48)	0.082	2.59 (0.40 − 20.64)	0.337	1.61 (0.59 − 5.24)	0.371
ΔADC_{skew}[§]								
at 2 weeks	0.49 (0.10 − 1.80)	0.289	0.86 (0.17 − 3.77)	0.846	0.85 (0.36 – 2.10)	0.715	0.90 (0.42 − 1.95)	0.791

at 4 weeks	0.18 (0.02 − 0.89)	0.034	0.68×10^{-2} (7.32×10^{-6} − 0.23)	0.001	3.68 (1.04 – 17.27)	0.043	3.21 (1.04 − 11.26)	0.042
at 8 weeks	0.10 (0.05×10^{-1} − 0.81)	0.028	0.05 (3.53×10^{-5} − 1.72)	0.117	2.56 (0.54 − 17.87)	0.254	1.53 (0.64 − 4.38)	0.361
ADC_{kurt}[§]								
at baseline	1.69 (0.76 − 5.31)	0.208	1.79 (0.65 − 10.34)	0.310	0.89 (0.46 – 1.38)	0.641	0.98 (0.53 − 1.52)	0.939
at 2 weeks	1.64 (0.55 − 5.50)	0.379	0.87 (0.23 − 3.14)	0.828	1.02 (0.51 − 1.98)	0.947	0.57 (0.27 − 1.16)	0.123
at 4 weeks	0.55 (0.17 − 1.27)	0.176	0.06 (0.94×10^{-3} − 0.43)	<0.001	2.07 (1.23 – 3.56)	0.008	1.31 (0.81 − 2.04)	0.263
at 8 weeks	0.51 (0.09 − 2.15)	0.364	0.17 (0.61×10^{-2} −	0.124	1.13 (0.30 – 3.85)	0.850	0.75 (0.29 − 1.75)	0.506

					1.58)			
ΔADC_{kurt}[§]								
at 2 weeks	0.87 (0.45 − 1.56)	0.632	0.71 (0.25 − 1.44)	0.388	1.08 (0.77 – 1.69)	0.691	0.86 (0.63 − 1.29)	0.430
at 4 weeks	0.59 (0.26 − 1.06)	0.079	0.28 (0.06 − 0.71)	0.003	1.57 (1.05 – 2.41)	0.028	1.15 (0.82 − 1.61)	0.418
at 8 weeks	0.79 (0.31 − 1.78)	0.572	0.65 (0.13 − 2.22)	0.512	0.74 (0.42 – 1.39)	0.345	0.74 (0.45 − 1.24)	0.245

Data are expressed as odds ratio or hazard ratio (95% confident interval). Univariate logistic regression analyses were used for objective response and disease controls. Univariate Cox proportional hazard analyses was used for progression-free and overall survival. Only significant factors are shown in this table, and results of the other non-significant factors are shown in Supplementary Table 2.

ADC, apparent diffusion coefficient; ADC_{kurt}, kurtosis of ADC; ADC_{skew}, skewness of ADC; N.E.; not estimated; PD-L1, programmed cell death-ligand 1; TPS, tissue proportion score; Δ, change from the baseline.

[∫]per $1\times10^{-3}mm^2$/sec increase

[§]per 1 increase

Table 3. Comparison of changes in skewness of ADC and responses according to RECIST at 4 weeks in each case

Case	ΔADC_{skew} at 4 weeks	RECIST at 4 weeks	Overall response
No. 1	Not decreased	PD	PD
No. 2	Not decreased	SD	SD
No. 3	Not decreased	SD	SD
No. 4	Decreased	SD	SD
No. 5	Not decreased	SD	PD
No. 6	Not decreased	SD	PD
No. 7	Decreased	SD	PR
No. 8	Not decreased	SD	SD
No. 9	Not decreased	PD	PD
No. 10	Decreased	PD (pseudoprogression)	PR
No. 11	Decreased	PD (pseudoprogression)	PR
No. 12	Decreased	PD (pseudoprogression)	PR
No. 13	Decreased	SD	PR

No. 14	Not decreased	SD	PD
No. 15	Decreased	PR	PR
No. 16	Decreased	SD	SD
No. 17	Decreased	SD	PR
No. 18	Decreased	SD	PR
No. 19	Decreased	PR	PR
No. 20	Decreased	SD	SD

ADC, apparent diffusion coefficient; CR, complete response; PD, progressive disease; PR, partial response; RECIST, Response Evaluation Criteria in Solid Tumors; SD, stable disease; ΔADC_{skew}, change in skewness of ADC from the baseline. The cutoff value of decreased ΔADC_{skew} was −0.01, determined by ROC analysis for the objective response.

Supplementary File

Supplementary Table 1. Results of IVIM-MRI measurements

Variables	All patients, n=20	PD, n=5	SD, n=6	PR, n=9
ADC, $\times 10^{-3} mm^2/sec$				
at baseline	1.39 (1.06 − 2.76)	1.50 (1.25 − 1.87)	1.46 (1.16 − 1.97)	1.28 (1.06 − 2.76)
at 2 weeks	1.47 (1.01 − 2.14)	1.54 (1.11 − 1.79)	1.44 (1.10 − 1.79)	1.40 (1.01 − 2.14)
at 4 weeks	1.40 (0.92 − 2.00)	1.38 (1.09 − 1.42)	1.49 (1.16 − 1.42)	1.55 (0.92 − 2.00)
at 8 weeks	1.63 (0.95 − 2.89)	1.46 (1.34 − 1.59)	1.55 (1.02 − 1.96)	1.73 (0.95 − 2.89)
ΔADC, $\times 10^{-3} mm^2/sec$				
at 2 weeks	0.03 (-0.82 − 0.80)	0.02 (-0.275 − 0.295)	0.04 (-0.38 − 0.17)	0.03 (-0.82 − 0.80)
at 4 weeks	0.02 (-1.00 − 0.51)	-0.235 (-0.50 − 0.14)	0.19 (-0.12 – 0.23)	0.07 (-1.00 − 0.51)
at 8 weeks	0.07 (-0.54 – 0.64)	-0.30 (-0.54 − -0.07)	-0.03 (-0.44 – -0.37)	0.31 (-0.28 − 0.64)
ADC_{skew}				
at baseline	0.50 (-0.52 − 2.08)	0.40 (0.14 − 0.60)	0.14 (-0.21 − 0.92)	0.85 (-0.52 − 2.08)
at 2 weeks	0.33 (-0.73 − 1.17)	0.19 (-0.51 − 0.93)	0.29 (-0.51 − 0.81)	0.37 (-0.73 − 1.17)
at 4 weeks	0.22 (-0.58 − 1.00)	0.79 (0.50 − 1.00)	-0.40×10^{-2} (-0.58 − 0.29)	0.12 (-0.53 − 0.65)
at 8 weeks	0.11 (-1.24 − 0.96)	0.54 (0.12 − 0.96)	0.07 (-0.14 – 0.43)	0.03 (-1.24 − 0.63)

Supplementary File

ΔADC_{skew}				
at 2 weeks	-0.30 (-1.92 − 1.02)	-0.30 (-1.11 − 0.60)	0.04 (-0.71 − 1.02)	-0.33 (-1.92 − 0.89)
at 4 weeks	-0.17 (-1.56 − 0.72)	0.39 (0.01 − 0.72)	-0.35 (-1.03 − 0.50)	-0.46 (-1.56 − -0.01)
at 8 weeks	-0.17 (-1.93 − 0.50)	0.17 (-0.01 − 0.36)	0.02 (-1.06 − 0.50)	-0.65 (-1.93 − 0.02)
ADC_{kurt}				
at baseline	3.64 (2.85 − 8.05)	3.32 (2.98 − 5.41)	3.89 (3.06 − 4.69)	3.71 (2.85 − 8.05)
at 2 weeks	3.81 (2.55 − 5.21)	4.26 (2.62 − 4.65)	3.25 (2.71 − 4.62)	4.15 (2.55 − 5.21)
at 4 weeks	3.50 (2.32 − 7.53)	4.76 (3.98 − 7.53)	3.10 (2.63 − 3.91)	3.41 (2.32 − 4.67)
at 8 weeks	3.08 (2.17 − 4.63)	3.98 (3.32 − 4.63)	2.98 (2.50 − 4.39)	3.07 (2.17 − 4.22)
ΔADC_{kurt}				
at 2 weeks	0.10 (-5.07 − 1.66)	0.69 (-2.79 − 1.66)	-0.07 (-1.97 − 0.44)	-0.32 (-5.07 − 1.50)
at 4 weeks	-0.45 (-4.57 − 3.96)	1.44 (-0.84 − 4.00)	-0.45 (-1.78 − -0.08)	-0.90 (-4.57 − 1.82)
at 8 weeks	-0.76 (-3.68 − 1.64)	-0.22 (-2.08 − 1.64)	-0.49 (-1.91 − 0.27)	-0.80 (-3.68 − 0.80)
D, mm^2/sec				
at baseline	1.06 (0.70 − 3.56)	1.22 (0.99 − 1.54)	1.09 (0.95 − 1.95)	0.94 (0.70 − 3.56)
at 2 weeks	1.11 (0.71 − 1.74)	1.14 (0.93 − 1.41)	1.05 (0.71 − 1.51)	1.13 (0.74 − 1.74)
at 4 weeks	1.07 (0.16 − 1.56)	1.02 (0.70 − 1.19)	1.15 (0.81 − 1.22)	0.98 (0.16 − 1.56)

at 8 weeks	1.30 (0.69 − 2.74)	1.20 (1.10 − 1.31)	1.15 (0.74 – 1.44)	1.35 (0.69 − 2.74)
Δ*D*, mm^2/sec				
at 2 weeks	-0.03 (-1.82 − 0.47)	-0.13 (-0.15 − 0.15)	-0.13 (-0.45 − 0.06)	0.14 (-1.82 − 0.47)
at 4 weeks	-0.01 (-3.40 − 0.50)	-0.04 (-0.56 − 0.12)	-0.01 (-0.78 − 0.17)	0.14 (-3.40 − 0.50)
at 8 weeks	0.07 (-0.82 – 0.74)	-0.17 (-0.44 − 0.09)	-0.12 (-0.52 – 0.33)	0.31 (-0.82 − 0.74)
*D**, mm^2/sec				
at baseline	64.26 (18.04 – 1.73×10^2)	67.26 (43.67 − 1.73×10^2)	59.30 (39.24 − 88.32)	78.62 (18.04 − 1.63×10^2)
at 2 weeks	52.59 (9.69 − 163.39)	73.63 (53.29 − 1.28×10^2)	38.43 (9.69 − 81.37)	40.86 (23.58 − 1.63×10^2)
at 4 weeks	45.58 (20.13 − 116.85)	46.70 (28.90 − 91.11)	51.74 (20.13 − 76.57)	44.46 (22.02 − 1.17×10^2)
at 8 weeks	49.68 (23.31 − 126.19)	98.64 (71.10 − 1.26×10^2)	49.68 (23.31 − 1.07×10^2)	31.29 (24.54 − 98.03)
Δ*D**, mm^2/sec				
at 2 weeks	-1.15 (-1.22×10^2 − 84.77)	29.96 (-1.03×10^{-2} – 58.88)	-19.05 (-60.89 − 24.04)	-0.89 (-1.22×10^{-2} – 84.77)

at 4 weeks	-19.86 (-97.06 − 44.09)	-19.17 (-97.06 − 21.45)	-15.02 (-25.35 − 15.31)	-32.70 (-56.99 − 44.09)
at 8 weeks	5.48 (-73.85 − 76.06)	39.95 (3.84 − 76.06)	8.33 (-47.27 − 49.45)	-19.79 (-73.85 − 69.17)
f, %				
at baseline	23.13 (11.10 − 54.00)	17.95 (11.10 − 34.25)	24.08 (17.25 − 32.60)	26.10 (17.80 − 54.00)
at 2 weeks	27.33 (16.25 − 48.30)	23.45 (16.25 − 30.05)	29.93 (24.75 − 45.15)	26.80 (17.15 − 48.30)
at 4 weeks	25.68 (11.05 − 69.20)	22.40 (11.05 − 40.75)	27.53 (19.40 − 44.60)	26.30 (14.10 − 69.20)
at 8 weeks	25.33 (13.85 − 60.15)	18.25 (16.60 − 19.90)	25.25 (20.90 − 37.65)	31.70 (13.85 − 60.15)
Δ*f*, %				
at 2 weeks	1.95 (-20.45 − 20.75)	1.70 (-5.15 − 12.35)	5.53 (-1.85 − 20.75)	1.35 (-20.45 − 11.7)
at 4 weeks	4.30 (-16.75 − 29.65)	4.30 (-16.75 − 29.65)	4.20 (-6.45 − 12.00)	4.30 (-15.70 − 15.20)

at 8 weeks	3.23 (-17.65 − 9.60)	-7.85 (-17.65 − 1.95)	4.28 (-8.50 − 6.65)	3.35 (-7.80 − 9.60)

Data are expressed as median (range)

ADC, apparent diffusion coefficient; ADC_{kurt}, kurtosis of ADC; ADC_{skew}, skewness of ADC; ECOG-PS, Eastern Cooperative Oncology Group performance status; N.E.; not estimated; PD-L1, programmed cell death-ligand 1; TPS, tissue proportion score; Δ, change from the baseline; *D*, true diffusion coefficient; *D**, pseudodiffusion coefficient; *f*, perfusion fraction.

Supplementary File

Supplementary table 2: Univariate logistic regression and Cox proportional hazard analyses of non-significant factors for the efficacy of immune checkpoint inhibitor therapy

	Objective response		Disease control		Progression-free survival		Overall survival	
Variables	Odds ratio	*p*-value	Odds ratio	*p*-value	Hazard ratio	*p*-value	Hazard ratio	*p*-value
Age								
≤65 years	1.00 (0.15 − 6.35)	1.000	1.00 (0.14 − 9.04)	1.000	1.14 (0.33 − 3.64)	0.832	0.81 (0.25 − 2.30)	0.705
≤75 years	0.40 (0.04 − 3.09)	0.377	0.55 (0.02 − 5.08)	0.618	1.36 (0.40 − 6.20)	0.639	0.91 (0.27 − 4.12)	0.884
Sex, male	2.67 (0.28 − 60.13)	0.411	3.25 (0.31 − 35.62)	0.310	0.43 (0.12 – 2.03)	0.259	0.57 (0.17 − 2.57)	0.420

Smoking, ever-smoker	4.00 (0.46 − 87.89)	0.211	2.00 (0.21 − 17.14)	0.526	0.36 (0.10 – 1.42)	0.135	0.40 (0.12 – 1.55)	0.172
ECOG-PS, 0 (vs. ≥1)	1.12 (0.19 − 6.59)	0.899	1.75 (0.25 − 15.57)	0.574	0.36 (0.08 − 1.27)	0.116	0.68 (0.21 − 1.94)	0.480
Stage, IIIb (vs. IV)	0.63 (0.03 − 7.73)	0.716	1.97×10^{7} (0.47 – N.E.)	0.137	0.65 (0.03 – 3.56)	0.668	0.41 (0.06 − 1.54)	0.207
Objective response at 4 weeks	5.97×10^{7} (0.85 – N.E.)	0.063	3.97×10^{7} (N.E.)	0.269	0.36×10^{-8} (N.E.)	0.999	0.31 (0.02 − 1.63)	0.266
ADC[∫]								
at baseline	0.88 (0.06 − 10.26)	0.917	0.79 (0.06 − 18.16)	0.862	1.38 (0.24 – 4.88)	0.674	0.71 (0.20 − 1.87)	0.513

at 2 weeks	1.05 (0.04 − 27.26)	0.974	0.57 (0.01 − 24.27)	0.760	1.75 (0.29 – 8.87)	0.517	1.28 (0.25 − 6.08)	0.759
at 4 weeks	1.53 (0.06 − 42.33)	0.791	12.68 (0.28 − 1.49×10^{3})	0.198	0.53 (0.06 – 4.40)	0.554	0.76 (0.15 − 3.69)	0.738
at 8 weeks	5.78 (0.59 − 1.60×10^{2})	0.140	2.75 (0.12 − 2.65×10^{2})	0.566	0.34 (0.05 – 1.75)	0.211	0.52 (0.14 – 1.52)	0.247
$D^{\#}$								
at baseline	1.07 (0.19 − 5.89)	0.926	1.03 (0.21 − 12.81)	0.974	1.05 (0.27 – 2.28)	0.929	0.65 (0.22 − 1.27)	0.240
at 2 weeks	1.42 (0.04 − 55.69)	0.843	0.28 (0.37×10^{-2} − 15.83)	0.524	3.18 (0.30 – 28.89)	0.323	0.64 (0.11 − 3.23)	0.598

at 4 weeks	0.40 (0.01 − 7.36)	0.532	1.22 (0.03 − 33.39)	0.905	1.35 (0.21 − 11.35)	0.765	2.85 (0.73 − 12.80)	0.135
at 8 weeks	7.24 (0.59 – 4.15×10^{2})	0.137	1.68 (0.09 – 1.80×10^{2})	0.768	0.30 (0.73×10^{-3} – 3.28)	0.208	0.41 (0.09 − 1.27)	0.135
$\Delta D^{\#}$								
at 2 weeks	0.99 (0.11 − 10.22)	0.990	0.57 (0.01 − 5.48)	0.666	1.43 (0.41 – 10.60)	0.639	1.98 (0.77 − 8.76)	0.182
at 4 weeks	0.84 (0.20 − 2.88)	0.757	1.01 (0.16 − 3.42)	0.983	1.02 (0.56 − 3.02)	0.961	1.53 (0.88 − 3.82)	0.148
at 8 weeks	6.56 (0.54 – 1.70×10^{2})	0.146	3.87 (0.10 – 3.04×10^{2})	0.460	0.26 (0.04 – 1.38)	0.114	1.26 (0.42 − 3.99)	0.678

*D** [#]								
at baseline	1.00 (0.98 − 1.02)	0.915	0.99 (0.97 − 1.02)	0.506	1.00 (0.99 – 1.02)	0.885	1.01 (0.99 − 1.02)	0.232
at 2 weeks	1.00 (0.97 − 1.02)	0.848	0.98 (0.94 − 1.00)	0.065	1.01 (0.99 – 1.02)	0.078	1.00 (0.99 − 1.01)	0.699
at 4 weeks	1.01 (0.97 − 1.04)	0.775	1.00 (0.96 − 1.04)	0.909	1.00 (0.98 – 1.02)	0.935	0.99 (0.97 − 1.01)	0.524
at 8 weeks	0.98 (0.95 − 1.01)	0.244	0.96 (0.87 − 1.01)	0.083	1.01 (0.99 – 1.04)	0.258	1.01 (0.99 − 1.03)	0.531
ΔD^* [#]								
at 2 weeks	1.00 (0.98 −	0.823	0.99 (0.97 −	0.368	1.01 (0.99 – 1.02)	0.167	1.00 (0.99 −	0.628

	1.02)		1.01)				1.01)	
at 4 weeks	1.00 (0.97 − 1.03)	0.927	1.01 (0.98 − 1.05)	0.462	1.00 (0.98 – 1.02)	0.788	0.98 (0.97 − 1.00)	0.070
at 8 weeks	0.99 (0.96 − 1.01)	0.376	0.98 (0.92 − 1.01)	0.179	1.01 (0.99 – 1.02)	0.476	1.00 (0.98 − 1.01)	0.704
f¶								
at baseline	1.08 (0.97 − 1.24)	0.150	1.17 (0.99 − 1.53)	0.056	0.96 (0.88 – 1.04)	0.362	0.97 (0.90 − 1.02)	0.209
at 2 weeks	0.99 (0.88 − 1.11)	0.905	1.12 (0.96 − 1.38)	0.154	0.98 (0.09 – 1.05)	0.546	1.03 (0.96 − 1.09)	0.438
at 4 weeks	1.01 (0.94 −	0.742	1.03 (0.95 −	0.518	0.99 (0.92 – 1.03)	0.574	0.97 (0.91 −	0.113

	1.09)		1.15)				1.01)	
at 8 weeks	1.08 (0.98 − 1.25)	0.130	1.34 (0.99 − 2.42)	0.054	0.98 (0.91 – 1.04)	0.602	0.98 (0.93 − 1.02)	0.317
Δf ¶								
at 2 weeks	0.90 (0.75 − 1.01)	0.083	0.97 (0.84 − 1.09)	0.591	1.01 (0.94 – 1.10)	0.758	1.07 (0.93 − 1.17)	0.063
at 4 weeks	0.97 (0.88 − 1.05)	0.426	0.97 (0.87 − 1.07)	0.532	1.00 (0.94 – 1.07)	0.933	0.96 (0.90 − 1.03)	0.261
at 8 weeks	1.09 (0.94 − 1.34)	0.267	1.19 (0.98 − 1.62)	0.080	0.94 (0.84 – 1.06)	0.289	0.95 (0.87 − 1.05)	0.329

Supplementary File

Data are expressed as odds ratio or hazard ratio (95% confident interval). Univariate logistic regression analyses were used for objective response and disease controls. Univariate Cox proportional hazard analyses was used for progression-free and overall survival. Only non-significant factors are shown in this table. ADC, apparent diffusion coefficient; ECOG-PS, Eastern Cooperative Oncology Group performance status; N.E., not estimated; Δ, change from the baseline; *D*, true diffusion coefficient; *D**, pseudodiffusion coefficient; *f*, perfusion fraction.

[∫] per 1×10^{-3} mm^2/sec increase

[#] per 1 mm^2/sec increase

[¶] per 1% increase

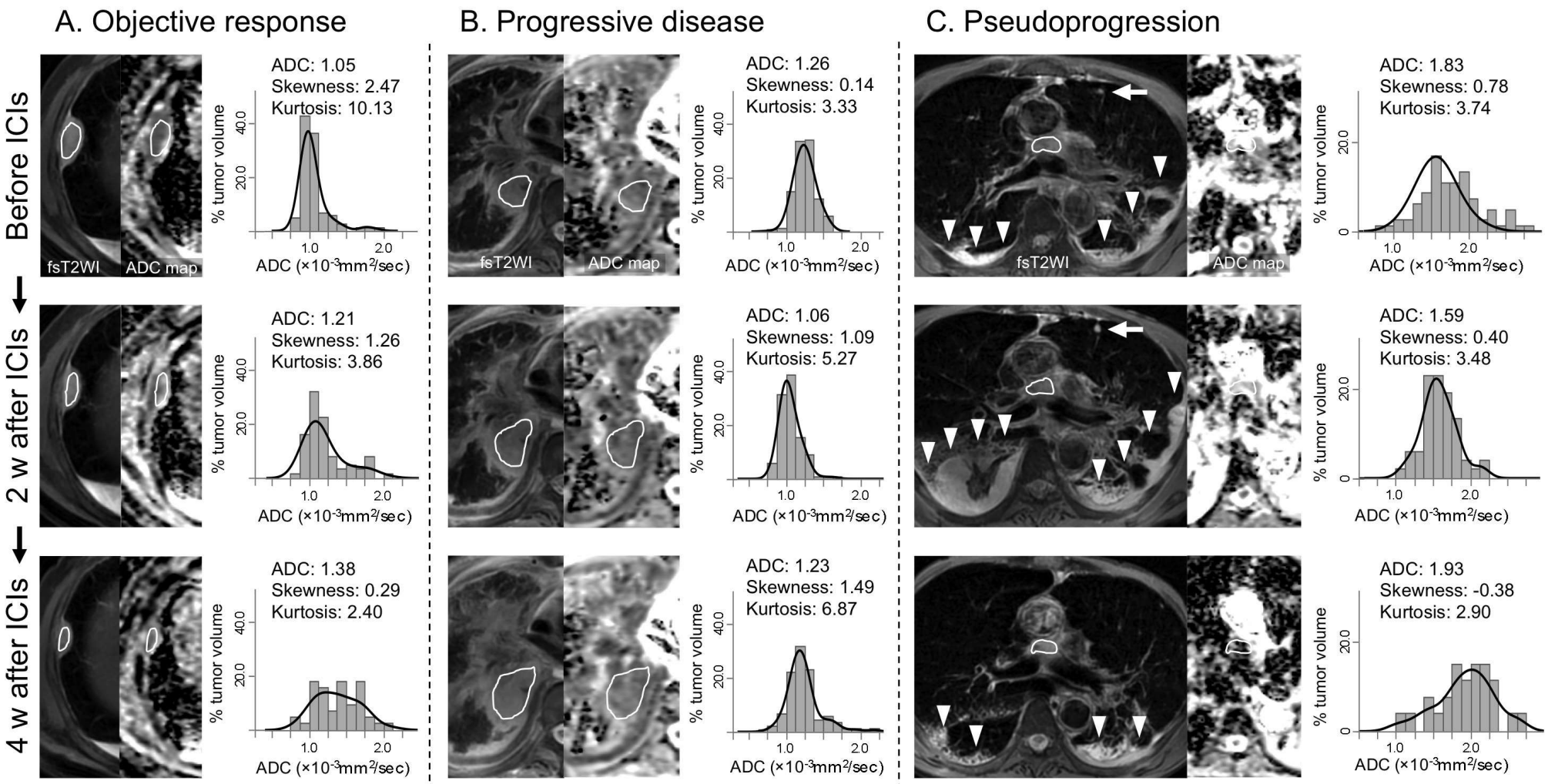
A. Objective response
B. Progressive disease
C. Pseudoprogression
Before ICIs
2 w after ICIs
4 w after ICIs
fsT2WI
ADC map
ADC: 1.05
Skewness: 2.47
Kurtosis: 10.13
ADC: 1.26
Skewness: 0.14
Kurtosis: 3.33
ADC: 1.83
Skewness: 0.78
Kurtosis: 3.74
ADC: 1.21
Skewness: 1.26
Kurtosis: 3.86
ADC: 1.06
Skewness: 1.09
Kurtosis: 5.27
ADC: 1.59
Skewness: 0.40
Kurtosis: 3.48
ADC: 1.38
Skewness: 0.29
Kurtosis: 2.40
ADC: 1.23
Skewness: 1.49
Kurtosis: 6.87
ADC: 1.93
Skewness: -0.38
Kurtosis: 2.90
% tumor volume
ADC (×10-3mm2/sec)

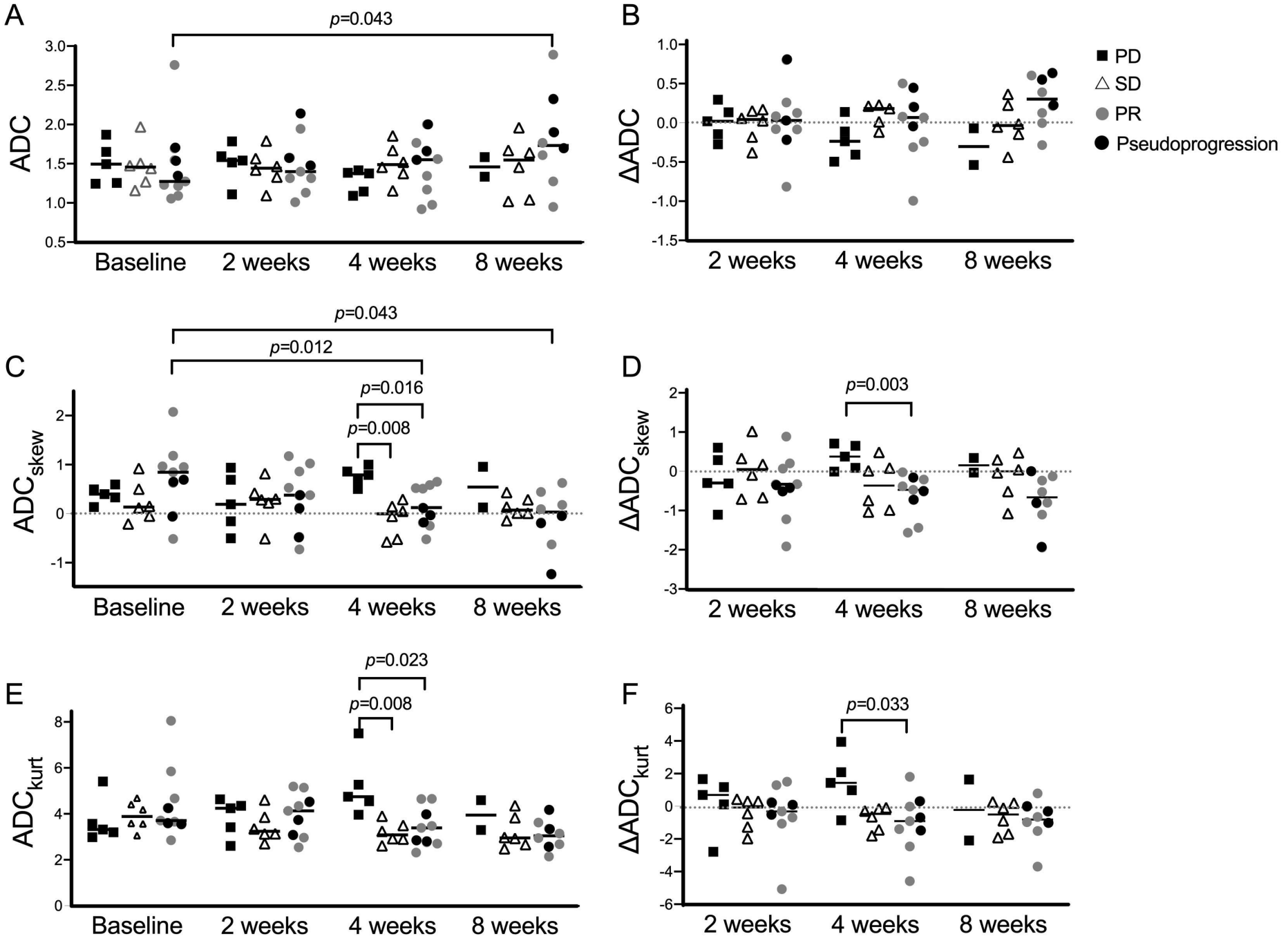
A
p=0.043
ADC
3.0
2.5
2.0
1.5
1.0
0.5
Baseline
2 weeks
4 weeks
8 weeks
B
ΔADC
1.0
0.5
0.0
-0.5
-1.0
-1.5
2 weeks
4 weeks
8 weeks
PD
SD
PR
Pseudoprogression
C
p=0.043
p=0.012
p=0.016
p=0.008
ADCskew
2
1
0
-1
Baseline
2 weeks
4 weeks
8 weeks
D
p=0.003
ΔADCskew
2
1
0
-1
-2
-3
2 weeks
4 weeks
8 weeks
E
p=0.023
p=0.008
ADCkurt
8
6
4
2
0
Baseline
2 weeks
4 weeks
8 weeks
F
p=0.033
ΔADCkurt
6
4
2
0
-2
-4
-6
2 weeks
4 weeks
8 weeks

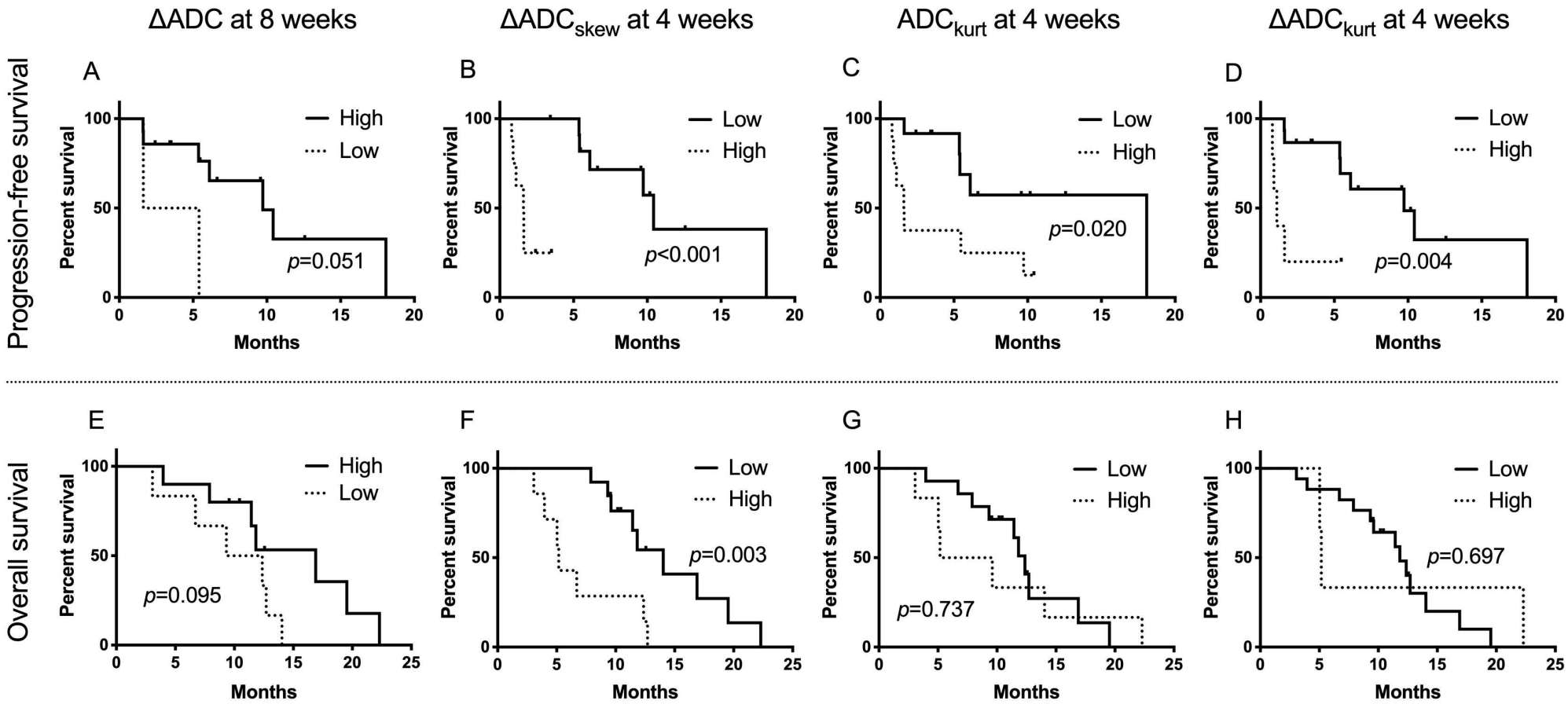
ΔADC at 8 weeks
ΔADC$_{skew}$ at 4 weeks
ADC$_{kurt}$ at 4 weeks
ΔADC$_{kurt}$ at 4 weeks
Progression-free survival
Overall survival
A
B
C
D
E
F
G
H
High
Low
Percent survival
Months
p=0.051
p<0.001
p=0.020
p=0.004
p=0.095
p=0.003
p=0.737
p=0.697